American Mineralogist, Volume 87, pages 269–276, 2002

Fibrous nanoinclusions in massive rose quartz: HRTEM and AEM investigations

CHI MA,* JULIA S. GOREVA,† AND GEORGE R. ROSSMAN

Division of Geological and Planetary Sciences, California Institute of Technology, Pasadena, California 91125, U.S.A.

ABSTRACT

Pink fibrous crystals within massive rose quartz from localities in California, South Dakota, Brazil, Madagascar, and Namibia were examined with high-resolution transmission electron microscopy (HRTEM) and analytical electron microscopy (AEM). This study reveals that the nanofibers in all samples are related to dumortierite. Selected-area electron diffraction (SAED) patterns and HRTEM images indicate that the dumortierite-related fibers have a superstructure with a doubled periodicity along the **a** and **b** axes of dumortierite, giving cell parameters $a = 2a_{dum} = 2.36$ nm, $b = 2b_{dum} = 4.05$ nm, $c = c_{dum} = 0.47$ nm. Computer simulations suggest that periodic arrangements of two different M1 site occupancies in the octahedral face-sharing chains give rise to the superstructure. One type of M1 site is occupied mainly by Al, whereas the other type is dominated by Ti and Fe. Simulated HRTEM images based on our proposed model match the experimental images. Most of the fibers, elongated along the **c** axis, are free of defects. AEM analysis shows that the dumortierite-related fibers have a composition similar to well-characterized dumortierite, but that they contain a greater amount of Fe substituting for Al in the M1 sites. Boron was detected in all fibers examined by electron energy loss spectroscopy as well as in sillimanite crystals found as a minor component in one rose quartz from Brazil.

INTRODUCTION

Fine fibers in massive rose quartz have been observed and, since the 1930s, were generally presumed to be rutile (reviewed by Rossman 1994 and Goreva et al. 2001). Applin and Hicks (1987) concluded that the fibrous phase in rose quartz from a Montana locality is dumortierite based on their TEM and powder X-ray diffraction (XRD) analyses. However, the XRD pattern produced by these fibers did not perfectly match that of dumortierite. Our XRD patterns of bulk fibers from rose quartz specimens from various localities also deviate from those of ideal dumortierite (Goreva et al. 2001). Significant differences observed in the IR and Raman spectra of these fibers cast additional doubt on their identification as dumortierite. These differences were the motivation for a more detailed TEM study of the fibers. Most fibers in massive rose quartz are less than 1 μm in thickness and are ideal for TEM examination (Fig. 1). Previously, the only published TEM observations on such fibers were those of Applin and Hicks (1987), who showed that the **c** axis repeat of the fibers from the Montana locality was appropriate for dumortierite. Detailed TEM studies of true dumortierite have also been very limited to date. Only van Dyck et al. (1976) have reported HRTEM observations on dumortierite (from Nevada) imaged along the [001] zone. Here we present a detailed analysis of the structural nature of individual fibers extracted from rose quartz based on HRTEM and AEM studies.

* E-mail: chi@gps.caltech.edu

† Current address: Department of Geological Sciences, Arizona State University, P.O. Box 871404, Tempe, Arizona 85287, U.S.A.

EXPERIMENTAL PROCEDURES

Samples

Rose quartz samples were selected from Madagascar (GRR1815), Olivera dos Brejinhos in western Bahia, Brazil (GRR1819), Joai'ma, Minas Gerais, Brazil (GRR1864), Rossing (not stated in the original sample description as received, but inferred from the sample), Namibia (GRR1818), Scott Mine, Custer, South Dakota (GRR1820), and Schindler Mine, Riverside County, California (GRR1996). All rose quartz samples are from pegmatite deposits. When examined at 400× with a light optical microscope, mineral inclusions were observed in only two of the samples selected for this study. In these two samples, numerous (GRR1864) and a few (GRR1819) needle-like crystals up to 10 μm in thickness are present.

Fibers were extracted from crushed quartz by dissolution in HF and then were concentrated and purified. More information on these specimens and the fiber purification procedure is given in Goreva et al. (2001). For comparison, detailed, parallel studies were conducted on a well-characterized blue dumortierite standard from Saharina, Madagascar (GRR347), studied by Moore and Araki (1978). Electron diffraction patterns were also obtained from pink dumortierite from Dehesa, San Diego County, California (GRR122), and blue dumortierite from the Cargo Muchacho Mountains, Imperial County, California (CIT14110).

Transmission electron microscopy

A JEOL atomic resolution microscope (ARM) operated at 800 kV and an in-situ JEOL 200CX TEM in the National Center for Electron Microscopy (NCEM), Lawrence Berkeley Laboratory (LBL), a Philips EM430 STEM operated at 300

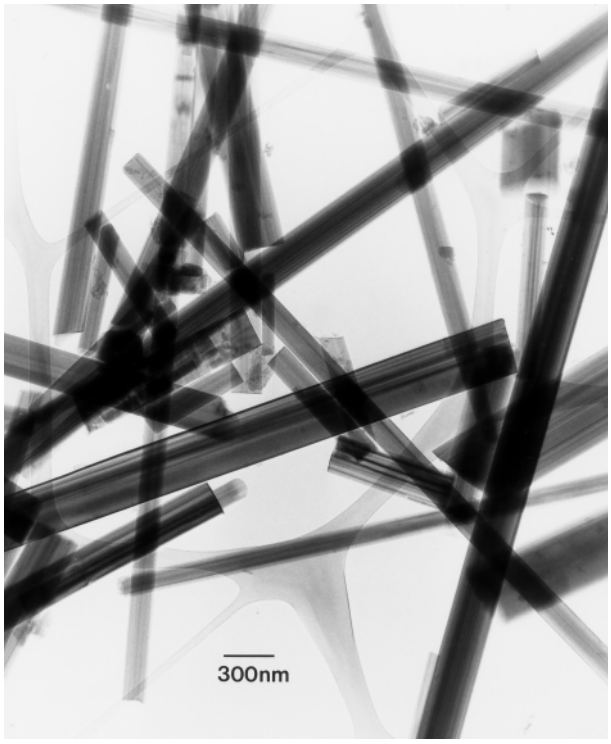

FIGURE 1. Low-magnification, bright-field image showing dispersed fibers on a carbon film. The fibers are from a rose quartz from Madagascar (GRR1815).

kV at Caltech, and an ISI TEM operated at 200 kV at the Jet Propulsion Laboratory were used for HRTEM imaging and/or electron diffraction analysis. AEM analysis was performed with a JEOL 200CX at the NCEM, LBL. The JEOL 200CX is equipped with a high-angle energy dispersive X-ray spectrometer (EDS) and a Gatan 666 electron energy loss spectrometer with parallel detection (PEELS) capable of routinely achieving 1.5 eV resolution. The *k* factors for the quantitative EDS analysis of the fibers were obtained using dumortierite, sillimanite, titanite, and andradite as standards under the same analytical conditions.

TEM specimens of the fibers were prepared in two ways: (1) crushed fiber particles were dispersed on a carbon film supported by a copper grid with the elongation of fibers parallel to the film and (2) sectioning of the fibers in resin with a diamond microtome to produce thin sections of the fibers normal to the electron beam. The dumortierite standard was prepared by dispersing crushed crystals on a carbon film. Because nearly 1000 photomicrographs were recorded during this study, we believe that our observations are representative.

HRTEM simulations

Computer simulations of HRTEM images and electron diffraction patterns were preformed using the NCEMSS (version 1.6) software package provided by Roar Kilaas. The input structure parameters for dumortierite (*Pmcn*, a = 1.1828 nm, b = 2.0243 nm, c = 0.47001 nm) and sillimanite (*Pbnm*, a = 0.7479 nm, b = 0.7670 nm, c = 0.5769 nm) were based on the data of Moore and Araki (1978) and Peterson and McMullan (1986), respectively. Two-dimensional structural images were simulated with the multislice approach for a typical range of microscope defocus values, crystal thicknesses, and crystal orientations, using a set of optical constants appropriate for the ARM, Philips EM430, and JEOL 200CX microscopes. The simulated and experimental images were compared visually for interpretation. Figure 2 illustrates computed HRTEM images of the dumortierite structure at different orientation, thickness, and defocus conditions. The simulations show that image details are highly sensitive to defocus, orientation, and the calculated range of specimen thickness. Hundreds of simulated images were generated in this study to assist in interpreting experimental atomic images.

Infrared spectroscopy

Infrared spectra were obtained using a Nicolet 860 Magna FTIR spectrometer and a SpectraTech Continuμm IR microscope. Sample preparation and operating conditions were similar to those reported in Goreva et al. (2001).

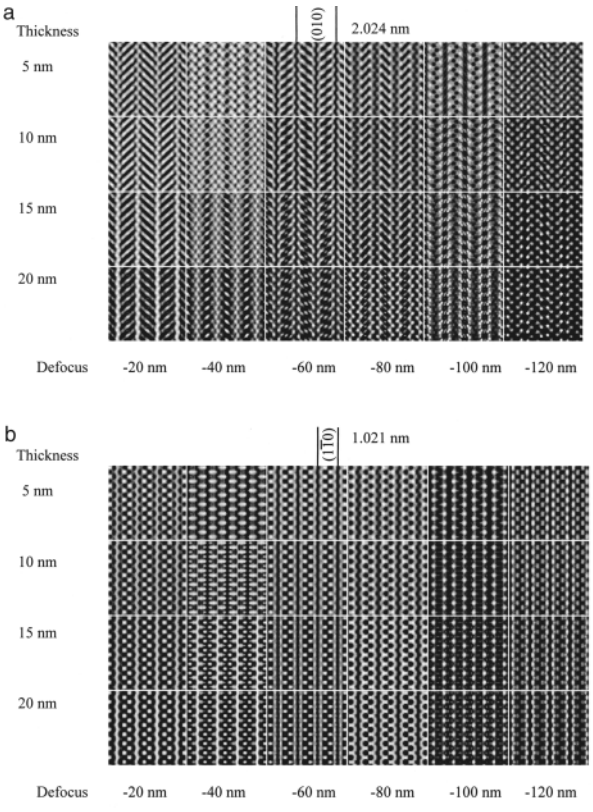

FIGURE 2. Simulated HRTEM images of dumortierite with different orientations and at different thickness and defocus conditions using optical constants for the Philips EM430. (**a**) [100] zone, (**b**) [110] zone.

RESULTS

Electron diffraction

Selected-area electron diffraction (SAED) patterns of the zone axes were obtained from a number of single-fiber crystals. Figure 3 shows representative zone axis SAED patterns of single fibers from rose quartz, compared with same zone axis patterns of the dumortierite standard. These SAED patterns are assigned to the [100], [010], [110], [111], and [001] zones based on a dumortierite structure model. The [010], [110], and [111] patterns were observed from the same areas of single fibers through tilting. The [100] zone axis pattern is almost identical to the dumortierite pattern. However, the [110] and [111] zone axis patterns of the fibers show weak but relatively sharp reflections halfway between the primary dumortierite reflections parallel to $[1\bar{1}0]^*$. This finding indicates that the fiber has a periodicity along $[1\bar{1}0]^* = 2d(1\bar{1}0)_{dum}$, which implies a superstructure of dumortierite with a doubled periodicity along both the **a** and the **b** axes (i.e., $a_{super} = 2a_{dum} = 2.38$ nm; $b_{super} = 2b_{dum} = 4.05$ nm). The [110] zone axis pattern of a fiber can be easily mistaken for a [100] zone pattern (Fig. 3a). However, the intensity distributions of the reflections are different. This superstructure was observed in rose quartz fibers from all localities examined. It was not observed in the ideal dumortierite samples.

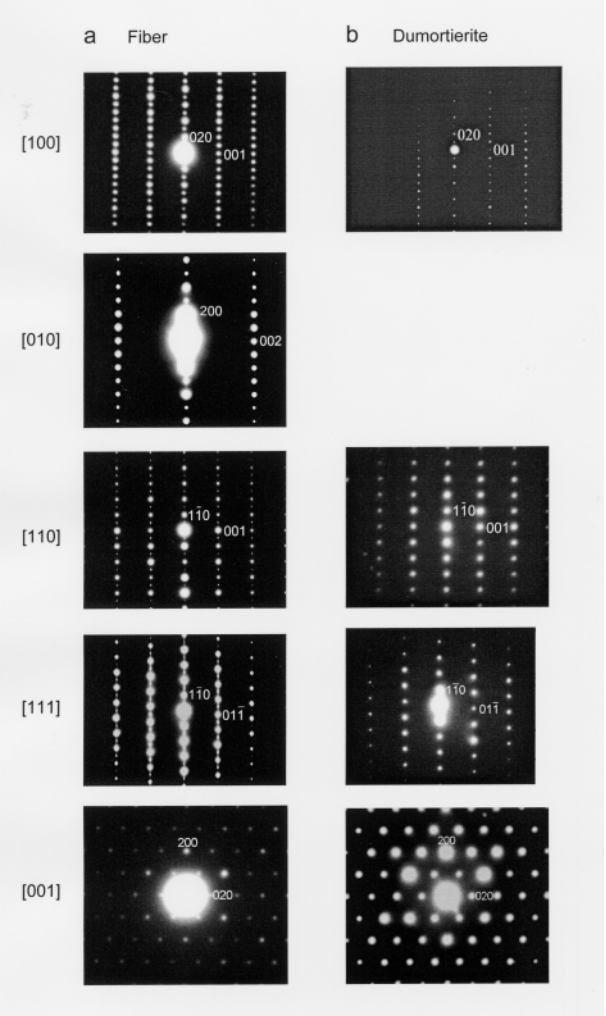

FIGURE 3. (**a**) Representative zone axis SAED patterns of single fibers obtained from different orientations: [100], [010], [110], [111], and [001]. (**b**) Zone axis SAED patterns of the dumortierite standard from [100], [110], [111], and [001]. All indices are based on the dumortierite structure determined by Moore and Araki (1978).

A series of electron diffraction patterns from a well-oriented dumortierite crystal were computed. The [100] zone axis patterns from a fiber and from the dumortierite standard (Fig. 3) are not well matched with the simulated [100] zone pattern of dumortierite as dynamical diffraction causes the presence of forbidden reflections such as (001) and (0k0) where $k = 2n + 1$ in the experimental SAED patterns.

The [001] zone-axis SAED patterns of the fibers and dumortierite are also similar and are matched closely with the simulated pattern of dumortierite and the experimental SAED pattern of dumortierite from the Rochester mining district, Nevada (van Dyck et al. 1976).

SAED patterns show that nearly all fibers in rose quartz have a superstructure of the dumortierite structure and are elongated along the **c** axis. A few [11l] zone single-crystal SAED patterns indicate that a very small number of fibers might have the ideal dumortierite structure because they exhibit no weak superstructure reflections along $[1\bar{1}0]^*$. Such patterns, however, might result from thin portions of the specimen foil where the superstructure information has weakened and/or has been damaged by the electron beam. The zone-axis SAED patterns of reference dumortierite (GRR347) examined in this study reveal that the dumortierite crystal has the ideal structure proposed by Moore and Araki (1978) (e.g., Fig. 3b). These patterns are consistent with the simulated dumortierite electron diffraction patterns.

Most SAED patterns of single-fiber crystals show sharp diffraction spots without diffuse streaking, indicative of long-range order. Only a few electron diffraction patterns revealing the superstructure show weak streaking (e.g., Fig. 3a) along $[1\bar{1}0]^*$. As is discussed below, the HRTEM images show that the streaking is derived not from stacking faults but from unequal cation occupancies in the M1 sites.

Convergent-beam electron diffraction patterns were also obtained from some dumortierite-related fibers. Figure 4 illustrates a [010] zone whole pattern of a fiber showing a weak first-order Laue zone (FOLZ) and a sharp second-order Laue zone (SOLZ). The FOLZ reveals that the repeat along [010] is 4.05 nm (i.e., the periodicity of the fiber along the **b** axis = $2b_{dum}$).

HRTEM imaging

Bright-field images at low-magnification reveal the morphology of the fibers (Fig. 1). In general, the fibers vary in thickness from 100 nm to 800 nm but can range up to 1200 nm.

HRTEM images indicate that the fibers are almost free of stacking faults, deformation, or dislocations. HRTEM images (Fig. 5) of single fibers corresponding to the orientation of the [110] and [112] zone SAED patterns (Fig. 3a) show that the true periodicity along the [110] direction is 2.04 nm; the subperiodicity of 1.02 nm appears only in thin regions of the foil.

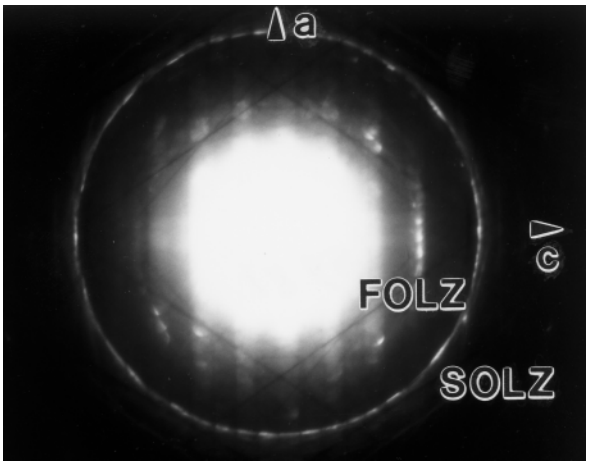

FIGURE 4. The [010] zone CBED pattern of a fiber from GRR1819 showing the First-Order Laue Zone (FOLZ) and the Second-Order Laue Zone (SOLZ).

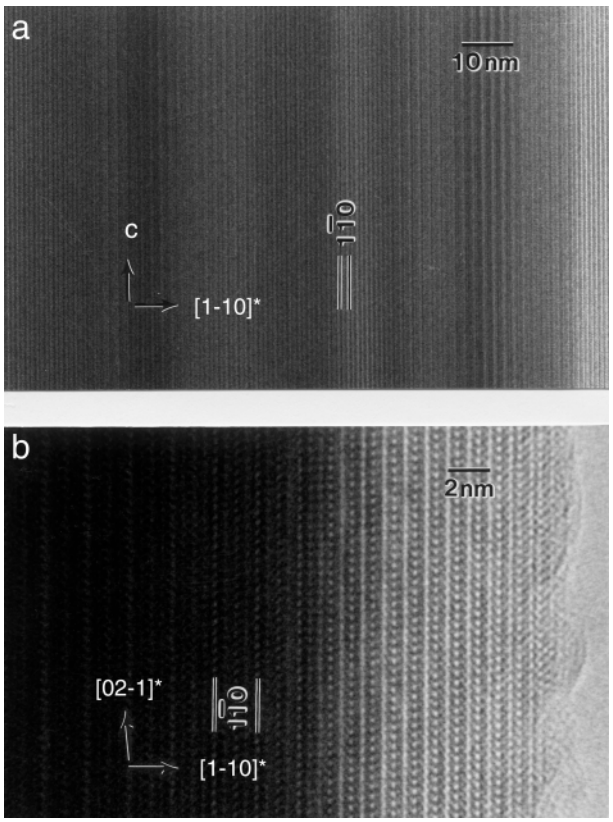

FIGURE 5. HRTEM images of single fibers showing 2.04 nm real-periodicity along the [110]* direction and 1.02 nm subperiodicity at a thinner area. (**a**) [110] zone, (**b**) [112] zone.

The [100] zone axis images (Fig. 6) show only the dumortierite-like sub-periodicity of 2.02 nm along [010]. Cross-sections of the fibers (Fig. 7) reveal (010), (100), (110), (130), and (140) crystal faces indexed according to the dumortierite superstructure. A likely (110) contact twin or stacking fault was observed in only one fiber.

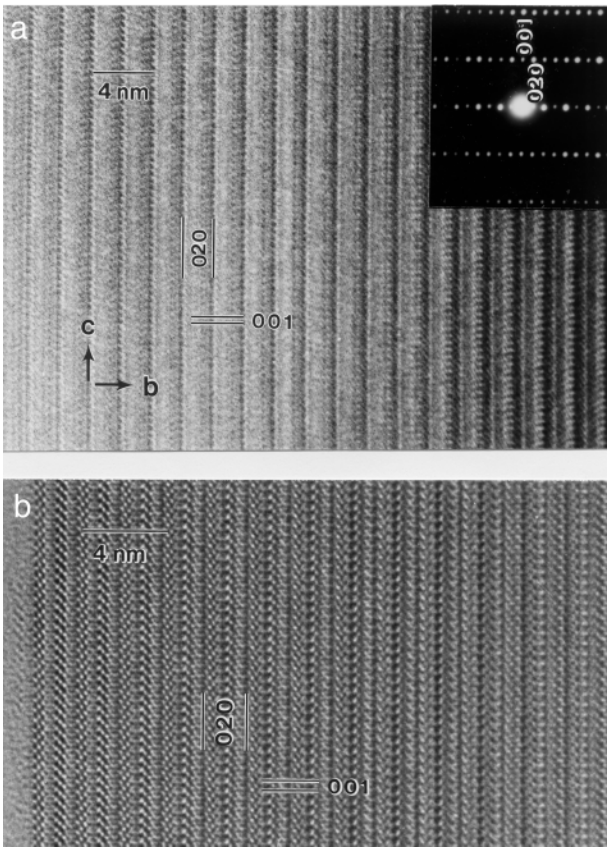

FIGURE 6. HRTEM images of single fibers down the [100] zone axis showing only subperiodicity along the [010] direction, such that $d(020)_{super} = b_{dum}$.

The irregular shape of the surface (<2 nm thick) of the fibers and the boundary between the crystalline and amorphous regions in Figure 5b are likely caused by electron beam damage. In general, electron beam damage on the fiber phase is not serious, although knock-on damage probably plays a role in degrading its structural ordering.

Chemical composition

AEM analyses of individual fibers show that in all samples the fibers from rose quartz are Al-borosilicates, having a chemical composition similar to dumortierite. Mean structural formulae of the fibers are given in Table 1. EDS analysis reveals that the fibers contain a small amount of Ti and Fe substituting for Al. The contents of Ti and Fe are slightly higher than in blue dumortierite (Fig. 8), but overlap the range of these elements reported in pink dumortierite (Alexander et al. 1986). In the fibers from rose quartz, the Ti content is generally greater than the Fe content. Ti and Fe are believed to occupy the M1 sites in dumortierite (Platonov et al. 2000).

Borate content. FTIR analyses of bulk, extracted fibers, including those used in this study, reveal that borate is present in about the same B to Si ratio as in dumortierite (Goreva et al. 2001). PEELS analysis reveals that B is present in each single

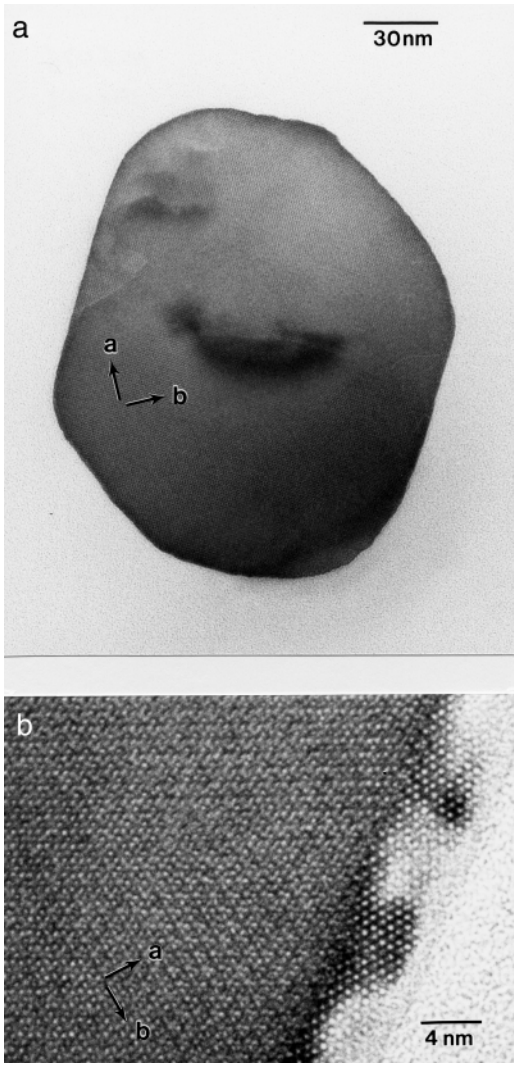

FIGURE 7. [001] zone axis HRTEM images of a fiber from GRR1815 showing its cross section.

TABLE 1. Mean chemical formula of the fibers in rose quartz and reference dumortierite by AEM (EDS) analysis

Sample no.	Locality	Dumortierite-related fibers*
GRR1815	Madagascar	$(Al_{6.71}Ti_{0.15}Fe_{0.13})Si_{3.00}BO_{18}$
GRR1818	Namibia	$(Al_{6.64}Ti_{0.17}Fe_{0.15})Si_{3.02}BO_{18}$
GRR1819	Bahia, Brazil	$(Al_{6.68}Ti_{0.17}Fe_{0.13})Si_{3.01}BO_{18}$
GRR1864	Minas Gerais, Brazil	$(Al_{6.58}Ti_{0.25}Fe_{0.09})Si_{3.02}BO_{18}$
GRR1996	Schindler Mine, CA	$(Al_{6.68}Ti_{0.17}Fe_{0.13})Si_{3.01}BO_{18}$
	Reference Dumortierite*	
GRR347	Saharina, Madagascar	$(Al_{6.86}Ti_{0.06}Fe_{0.06})Si_{3.02}BO_{18}$
	Sillimanite microcrystals†	
GRR1864	Minas Gerais, Brazil	$Al_{1.98}Fe_{0.02}Si_{1.00}O_5$

* Formulas are normalized to BO_{18}.
† Formula normalized to O_5.

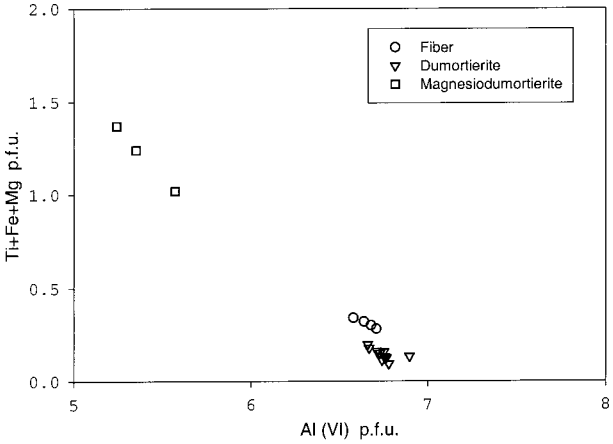

FIGURE 8. Octahedral cation contents in the fibers from rose quartz (this study), classic dumortierite (Alexander et al. 1986), and magnesiodumortierite (Chopin et al. 1995).

fiber from rose quartz (Fig. 9a). Although attempts to obtain reproducible quantitative PEELS analyses were, in part, frustrated by the irregular shape and thickness of the individual samples, these analyses also show that the B content of the fibers is similar to that of dumortierite (Fig. 9b).

Hydroxide-fluoride content. Electron microprobe analyses failed to reveal F in either the bulk fibers (GRR 1815) or dumortierite (GRR 347). Our FTIR analyses suggest that OH is present in the fibers at somewhat greater concentrations than observed in dumortierite. Figure 10 is a representative comparison of the OH absorption pattern of an unpolarized spectrum of a polycrystalline slab (c, $\perp$ c orientation) of pink (Dehesa) dumortierite and a mat of pink fibers (GRR 1815). Both samples show an additional but variable hydrous component at about 3240 cm^{-1} that we associate with contamination in the bulk samples. Spectroscopic differences between dumortierite and the fibers are apparent in the borate bands in the 2000 and 3200 cm^{-1} region. These differences are expected based on previously identified spectroscopic differences in the 450–2000 cm^{-1} range (Goreva et al. 2001). Because of scattering from the bulk fiber mats, the spectra of the mats have strongly sloping backgrounds. The spectrum of the fibers in Figure 11 was subjected to an arbitrary correction so that the samples have about the same slope between 4000 and 2000 cm^{-1}. In addition, because the effective spectroscopic thickness of the fiber mat could not be determined accurately, the spectra were scaled to have the same intensity at 2850 cm^{-1}. These arbitrary corrections render it impossible to establish the absolute concentration of OH in the fibers.

Other mineral fibers

In several recent books and articles (e.g., Manutchehr-Danai 2000 and Webster 1994), rutile fibers (TiO_2) are still cited as the cause of color in rose quartz. A control experiment with light-yellow, rutilated quartz (CIT 5585, Minas Gerais, Brazil) demonstrated that fine rutile needles (1.5 μm wide and whose

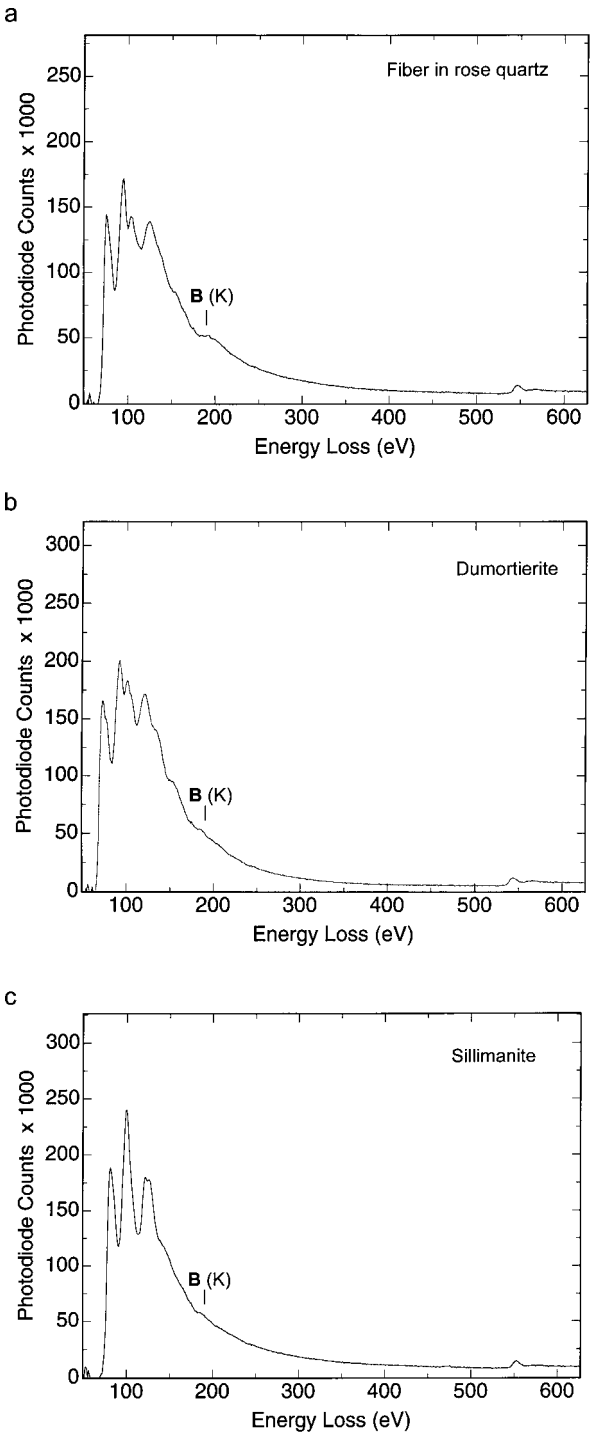

FIGURE 9. PEELS spectrum of (**a**) a dumortierite-related fiber (GRR1819), (**b**) the dumortierite standard (GRR347), and (**c**) a sillimanite nanocrystal (GRR1864). The B *K*-edge is evident in all spectra.

identity was verified by Raman spectroscopy) survive our acid dissolution process intact. Thus, if rutile fibers were present in rose quartz in significant numbers, we should detect them. However, rutile fibers were not found in any of our rose quartz

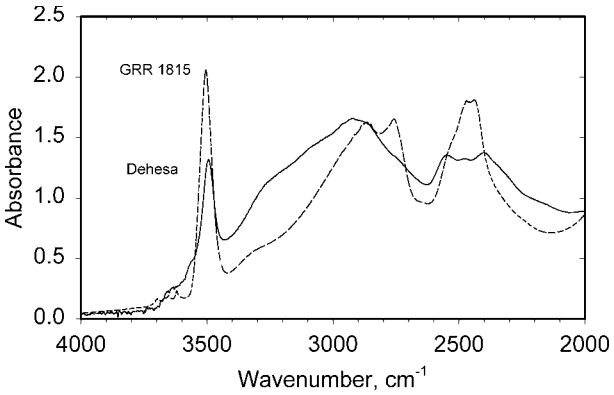

FIGURE 10. Comparison of infrared absorption spectrum taken through a mat of pink fibers (GRR 1815) and a polycrystalline slab of pink dumortierite (GRR122).

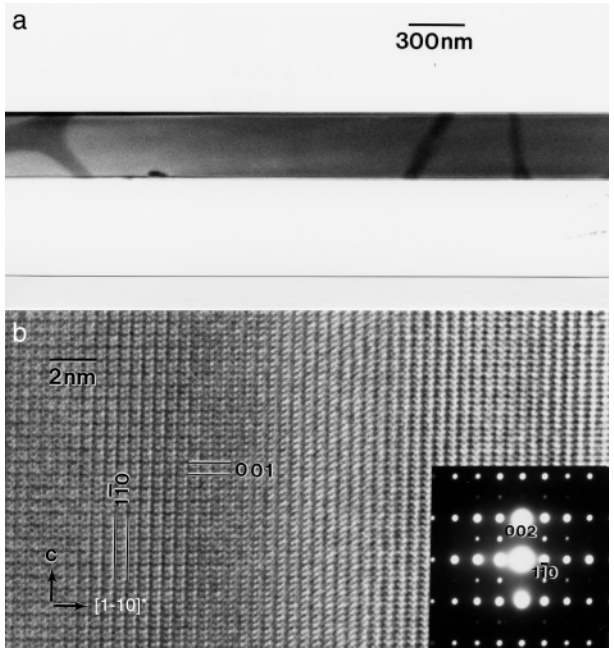

FIGURE 11. (**a**) A thin sillimanite crystal from GRR1864. (**b**) [110] zone axis HRTEM image of the sillimanite crystal from GRR1864 and its SAED pattern.

samples. Along with the dumortierite-related fibers, a significant proportion of acicular sillimanite nanocrystals (~10%) were admixed with the fibers extracted from one sample of Brazilian rose quartz (GRR1864). Figure 11 illustrates an HRTEM image of a sillimanite crystal with its [110] zone axis SAED pattern, which is closely matched to the calculated image and electron diffraction pattern. The composition of the sillimanite crystals corresponds almost exactly to Al_2SiO_5 (Table 1). Similar, but larger (up to 15 µm wide), acicular Al_2SiO_5 crystals were observed as a minor component in the SEM images of fibers extracted from samples GRR1819 and GRR1820 of Goreva et al. (2001) and were presumed also to be sillimanite.

PEELS analysis shows that B occurs in the sillimanite from

rose quartz (Fig. 9c). The B content appears not to be caused by contamination by dumortierite-related fibers, or inclusions in sillimanite of borosilicates. This result is consistent with a prior observation of B in macroscopic sillimanite (Grew and Rossman 1985). Although B has previously been recognized only as a trace element in sillimanite, we believe that a more significant amount of B may likely substitute for Al in our sillimanite. Because the PEELS spectra were obtained under different conditions (e.g., crystal thickness, orientation), rigorous quantitative analyses were not possible. However, the intensity of the B peak in the PEELS spectrum of sillimanite is similar to that of dumortierite. Because B is an essential component of dumortierite, this result might imply that the B content in sillimanite from rose quartz is comparably high. However, the normalized chemical analysis of Table 1 does not indicate a significant deviation from stoichiometry.

DISCUSSION

Experimental TEM results in this study indicate most fibers from rose quartz are a superstructure of dumortierite with a doubled periodicity along both the **a** and the **b** axes. The superstructure can be modeled based on a periodic variation of the M1 position in the dumortierite structure. The ideal dumortierite structure consists of three chain types (each built of AlO_6 octahedra) that run parallel to the **c** axis: an $^{1}_{\infty}[M1O_3]$ face-sharing chain, $^{1}_{\infty}(M4_4O_{12})$ double chains, and $^{1}_{\infty}(M2_2M3_2O_{12})$ chains (Moore and Araki 1978). The M2, M3, and M4 sites are occupied completely by Al. The M1 site is occupied mainly by Al and cation vacancies in a 3:1 ratio in normal dumortierite (Moore and Araki 1978), and by Mg in magnesiodumortierite (Chopin et al. 1995). The AEM analyses of individual fibers show the presence of Ti and Fe (Table 1). Alexander et al. (1986) assign these two cations to the M1 site in dumortierite. We suggest that Al, Fe, and Ti cations order over the M1 sites to generate two symmetrically distinct types. Type I is filled only with Al, and Type II contains Ti and Fe. On this crystal-chemical basis, a model for the superstructure is constructed, as illustrated in Figure 12. In this model, viewed down the [001] direction, the Type I site is surrounded by Type II sites along the [100], [110], and [010] directions of the dumortierite structure. The superstructure derives from the regular distribution of these two types of cation occupancies in the M1 site. In the superstructure unit, three quarters of the M1 sites are Type I (Al) and one quarter are Type II (Ti and Fe). The stoichiometry of this model, $[Al_6(Al_{0.75})^{I}(Ti,Fe)^{II}_{0.25}]Si_3BO_{18}$, comes close to predicting the experimentally determined composition of the fibers in Table 1. The model does not exclude minor amounts of Ti and Fe in the Type I Al position nor does it exclude cation vacancies in either the Type I or Type II cation sites.

The simulated electron diffraction patterns of this model ($Pbc2_1$, $a = 2.3656$ nm, $b = 4.0486$ nm, $c = 0.47001$ nm) match well with the experimental SAED patterns of the dumortierite-related fibers (Fig. 3a). The simulated HRTEM images also closely match the experimental images of the fibers (Fig. 13). These simulations indicate that the superstructure occurring in the fibers indeed has such a cation configuration.

The streaking along the $[1\bar{1}0]^*$ direction in some SAED patterns of single fibers might correspond to some cation disor-

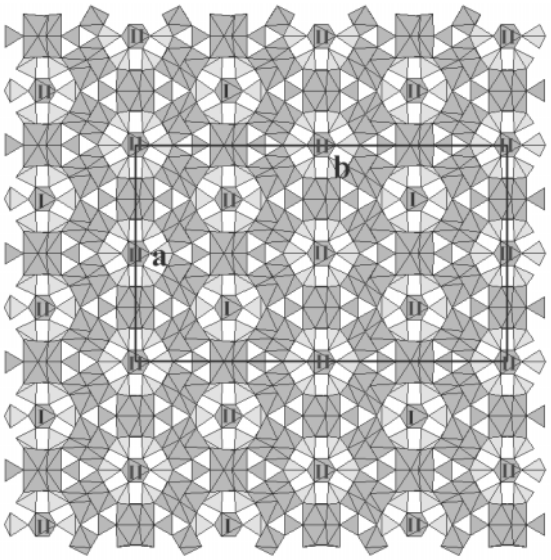

FIGURE 12. The superstructure model ($a = 2a_{dum}$, $b = 2b_{dum}$, $c = c_{dum}$). The superstructure is strongly pseudohexagonal, with **c** the pseudohexad axis. There are two types of M1 chain: Type I filled with Al, and Type II occupied by Ti and Fe.

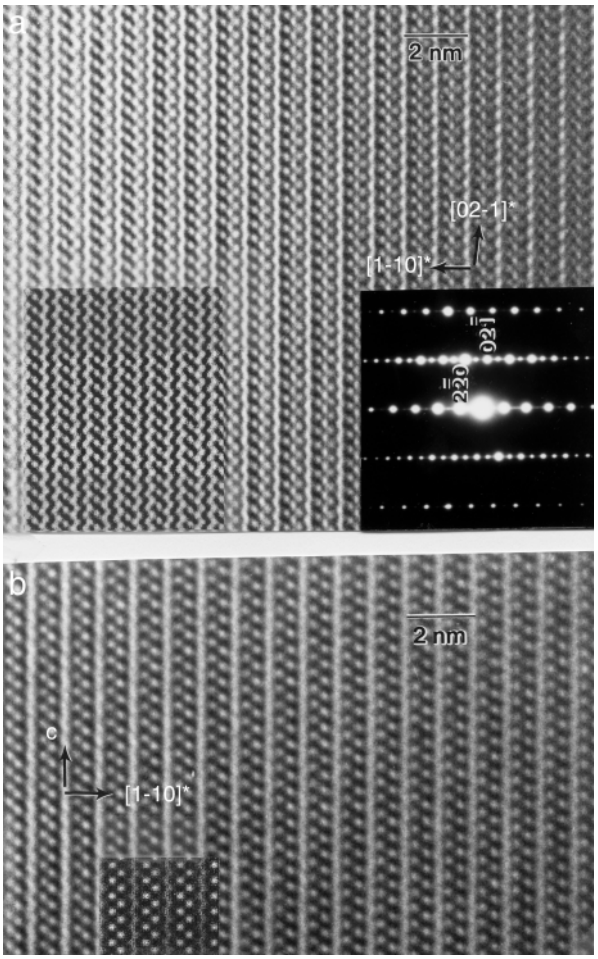

FIGURE 13. HRTEM images of single fibers viewed down the (**a**) [112] and (**b**) [110] directions, matched with the inserted simulated images using the superstructure model.

dering in the M1 sites. The chemistry of the fibers (Table 1) shows an average $Al_{0.66}Ti_{0.18}Fe_{0.13}$ per formula in the M1 site, which suggests that about 20% of the Ti and Fe are located in the Type I position with Al. It is likely that uneven distribution of Ti and Fe cations in the Type I position gives rise to the streaking along $[1\bar{1}0]^*$ in some of the fibers' SAED patterns.

It is apparent that Ti and Fe in the Type II position of the M1 site are disordered along the **c** axis, whereas Al in the Type I position is ordered in the M1 site or partly disordered if minor Ti, Fe, or vacancies are present in the Type I position along with Al. This model predicts that in the fibers $c = c_{dum} = 0.47$ nm without a doubled or tripled repetition, as is observed in the experimental electron diffraction results.

If Al, Ti, and Fe are randomly distributed in the M1 site along **c***, the dumortierite structure occurs. This might be the case for a few fibers whose [11*l*] SAED patterns are almost identical to these of ideal dumortierite crystals.

Our model indicates that the pink color of the fibers results from intervalence charge transfer between Fe^{2+} and Ti^{4+} in the M1 site. A similar mechanism has previously been proposed as the cause of pink color of dumortierite (Alexander et al. 1986; Platonov et al. 2000). Although the fibrous borosilicate phases observed by HRTEM may seem volumetrically insignificant in rose quartz (Goreva et al. 2001), they are crucial to the very definition of rose quartz. If the dumortierite-related fibers are cogenetic with sillimanite, then constraints could be placed on the temperature of formation of both rose quartz and the fibers. Although it is possible that the fine acicular sillimanite crystals extracted from GRR1864 are cogenetic with the dumortierite-like fibers, it is likely that the rose fibers form from exsolution, post-crystallization, under conditions unrelated to the formation of the larger sillimanite crystals microscopically observed in GRR1864, and in samples GRR1819 and GRR1820 of Goreva et al. (2001). These larger crystals more likely were incorporated (by capture) during the growth of the quartz. Ironically, the microscopically visible needles that previously captured the attention of many researchers may have no relationship to the origin of color of rose quartz.

These observations raise the question of whether the ordering we observe in the fibers is a result of growth at a lower temperature than usual for dumortierite. It is reasonable to expect that exsolved phases might display higher ordering than their directly crystallized counterparts because lower temperature formation generally leads to higher order. In this respect, it would be interesting to find a locality with multiple generations of dumortierite formed at different temperatures and examine the state of ordering in the mineral.

ACKNOWLEDGMENTS

We thank Ulrich Dahmen and Christian Kisielowski for allowing us to access the ARM and the JEOL 200CX microscopes at the National Center for Electron Microscopy, Lawrence Berkeley National Laboratory, Roar Kilaas for helping with the NCEMSS image simulation program, Chengyu Song for assisting with the ARM operation, and Thomas George for allowing us to use the ISI 200 kV HRTEM at the Jet Propulsion Laboratory. Lothar Jung (Quartz Technology, Inc.) provided samples for this study and several stimulating discussions in the early stages of this project. Rock H. Currier (Jewel Tunnel Imports) and Edward Swobota (Beverly Hills, CA) also provided samples that were critical for this study. Careful reviews by Peter Heaney and Mike Zolensky led to a significant improvement in the quality of the manuscript. Primary funding for this project was provided by the White Rose Foundation with additional funding from the National Science Foundation through grant NSF EAR-9804871.

REFERENCES CITED

Alexander, V.D., Griffen, D.T., and Martin, T.J. (1986) Crystal chemistry of some Fe- and Ti-poor dumortierites. American Mineralogist, 71, 786–794.

Applin, K.R. and Hicks, B.D. (1987) Fibers of dumortierite in quartz. American Mineralogist, 72, 170–172.

Chopin, C., Ferraris, G., Ivaldi, G., Schertl, H.-P., Schreyer, W., Compagnoni, R., Davison, C., and Davis, A.M. (1995) Magnesiodumortierite, a new mineral from very-high-pressure rocks (western Alps). II. Crystal chemistry and petrological significance. European Journal of Mineralogy, 7, 525–535.

Goreva, J., Ma, C., and Rossman, G.R. (2001) Fibrous nanoinclusions in massive rose quartz. The source of rose coloration. American Mineralogist, 86, 466–472.

Grew, E.S. and Rossman, G.R. (1985) Co-ordination of boron in sillimanite. Mineralogical Magazine, 49, 132–135.

Manutchehr-Danai, M. (2000) Dictionary of gems and gemology, 565 p. Springer, N.Y.

Moore, P.B. and Araki, T. (1978) Dumortierite, $Si_3B[Al_{6.75}\square_{0.25}O_{17.25}(OH)_{0.75}]$: A detailed structural analysis. Neues Jahrbuch fur Mineralogie Abhandlungen, 132, 231–241.

Peterson, R.C. and McMullan, R.K. (1986) Neutron diffraction studies of sillimanite. American Mineralogist, 71, 742–745.

Platonov, A.N., Langer, K., Chopin, C., Andrut, M., and Taran, M.N. (2000) Fe^{2+}-Ti^{4+} charge transfer in dumortierite. European Journal of Mineralogy, 12, 521–528.

Rossman, G.R. (1994) Colored varieties of the silica minerals. In Heaney, P.J., Prewitt, C.T., and Gibbs, G.V., Ed., Silica Physical Behaviour, Geochemistry and Materials applications, 29, 433–467. Reviews in Mineralogy, Mineralogical Society of America, Washington, D.C.

van Dyck, D., Tambuyser, P., van Landuyt, J., and Amelinckx, S. (1976) High-resolution electron microscopy of dumortierite. American Mineralogist, 61, 1016–1019.

Webster, R. (1994) Gems: their sources, descriptions, and identification, 1026 p. 5th ed. Revised by P.G. Read. Butterworth-Heinemann, Oxford, U.K.

MANUSCRIPT RECEIVED APRIL 4, 2001
MANUSCRIPT ACCEPTED NOVEMBER 12, 2001
MANUSCRIPT HANDLED BY ADRIAN J. BREARLEY